Sixth International Symposium on Turbulence and Shear Flow Phenomena
Seoul, Korea, 22-24 June 2009

EXPERIMENTS ON THE LATE STAGES OF BOUNDARY LAYER TRANSITION

K V Manu, Joseph Mathew, J. Dey
Department of Aerospace Engineering,
Indian Institute of Science
Bangalore 560012 INDIA

manu@aero.iisc.ernet.in, joseph@aero.iisc.ernet.in, jd@aero.iisc.ernet.in

ABSTRACT

Experiments were conducted with two, smooth hills, lying well within the boundary layer over a flat plate mounted in a wind tunnel. One hill was shallow, with peak height $h = 1.5$ mm and width $C = 50$ mm; the other, steep, with $h = 3$ mm, $C = 30$ mm. Since the hills occupied one-half of the tunnel span, streamwise vorticity formed near the hills' edge. At a freestream speed of 3.5 m/s, streaks formed, with inflectional wall-normal and spanwise velocity profiles, but without effecting transition. Transition, observed at 7.5 m/s, took different routes with the two hills. With the steep hill streamwise velocity signals exhibited the passage of a wave packet which intensified before breakdown to turbulence. With the shallow hill there was a broad range of frequencies present immediately downstream of the hill. These fluctuations grew continuously and transition occurred within a shorter distance.

INTRODUCTION

A common feature of wall-bounded flows undergoing transition to turbulence is the presence of streamwise vortices. We should then consider the possibility that, in any route to transition, a point of no return occurs when there is an instability of these vortices. With this premise, Hamilton and Abernathy (1994) conducted experiments in a water table flow in which isolated streamwise vortices were generated by the side of a shallow hill. An objective was to distinguish between flows that would transition from those that would not, and to find a quantitative criterion. A threshold vortex strength was expected from earlier qualitative studies with the same facility. Accordingly, with their quantitative data (LDV measurements), a vortex Reynolds number $\mathrm{Re}_v = \Gamma/\nu$ was constructed from the circulation Γ in a crossflow plane (ν is the viscosity). They posited Re_v to be greater than some critical value as a requisite for transition, but found the upstream value of Re_v of transitional flow to be smaller than those for non-transitional cases. They offered a reconciliation with an *ad hoc* definition that distinguishes between circulation due to a vortex and circulation due to vorticity. Still, their novel and important study, which documented the role of isolated vortices and showed that transition does not always follow the appearance of inflectional profiles, remains inconclusive about a transition criterion. The present work is an examination of the role of such isolated vortices in transition of flat plate boundary layers.

Many routes to transition in wall-bounded flows have been observed in studies that span almost a century. It can begin from instability to small perturbations, followed by secondary instabilities; freestream disturbances outside a boundary layer can selectively perturb the flow within, which then undergoes transition; perturbations at the wall, such as roughness, suction or injection, may get amplified. In every case, the disturbance must become three-dimensional, as shown first by Klebanoff et al (1962), and suffer further instability, before transition occurs. A characteristic feature of this late three-dimensional stage is the prevalence of streamwise vortices and streamwise streaks. The subsequent breakdown is very fast and has no less rich a structure than the turbulent flow itself, that it is difficult to identify any distinct stages or processes. However, the prior stage, with streamwise vortices/streaks, is more tractable and has been the subject of several studies.

In the classical descriptions of boundary layer transition of the K or N (also called H) types, streamwise vortices appear as pairs connected by a head, also termed hairpin vortices (see, for example, the review by Kachanov, 1994). This structure is also seen near walls in fully turbulent flows. Streamwise elongated high- and low-speed streaks are dominant in bypass transition induced by freestream turbulence (see, for example, reviews by Saric et al, 2002; Durbin and Wu, 2007). Wall protuberances inevitably give rise to pairs of counter-rotating streamwise vortices. They form as horseshoe vortices about the windward side, but also shed as hairpins into the wake (Acarlar and Smith, 1987). Such vortex pairs cause high speed fluid to be brought close to the wall and low speed fluid to move away. In turn, streamwise velocity profiles acquire inflections in their variations in both spanwise and wall-normal directions. Since inflectional profiles are susceptible to inviscid instability, it has been thought that such a modification to the streamwise flow and its inviscid instability are essential, or at least common, precursors to transition. The experiments of Swearingen and Blackwelder (1987), Bakchinov et al (1995), and, Asai et al (2002) all seek to establish inflectional instability, especially with respect to the spanwise variation of the streamwise velocity profile, as a common precursor. Yet, vortex pairs are not necessary to create inflectional profiles; the action of a single vortex will suffice. Also, while inflectional profiles were observed in flows that underwent transition, there had been no reports of flows that had inflections but did not transition. Hamilton and Abernathy (1994) noted that an inflectional profile is not sufficient for instability, and showed from their experiments that inflectional profiles could be formed by the action of isolated vortices in flows that did not transition.

In this study half-span hills were embedded in the boundary layer on a flat plate, similar to the hill in the water table flow of Hamilton and Abernathy (1994). Experiments at two freestream speeds reveal characteristics of transitional and non-transitional flows with isolated streamwise vortices.

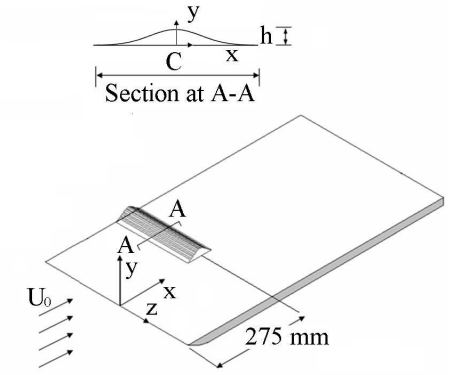

Figure 1: Experiment configuration

Table 1: Hill parameters

Hill shape	Chord C mm	Max. height mm	a
Shallow	50	1.5	10
Steep	30	3	7.1

DESCRIPTION OF EXPERIMENTS

The experiments were carried out in a low turbulence wind tunnel, the details of which are reported in Vasudevan et al (2001) and Banerjee et al (2006). Briefly, this is an open circuit tunnel with a square test section of dimensions 500 × 500 × 3000 mm. The settling chamber ahead of the contraction has a smooth entry section with honeycomb and screens (4 screens; 8 mesh wires/cm). The contraction ratio was 14:1, and its shape ensured a monotonic velocity increase. The tunnel has a short diffuser which was isolated from the rest of the tunnel by a flexible rubber band to minimize the transmission of vibrations to the test section. The tunnel speed was controlled by a speed controller that regulated a 5 KW DC motor, which drove the fan at the diffuser end. The maximum tunnel speed is 22 m/s, and the freestream turbulence level is about 0.05% for air speed below 10 m/s. The test section has a divergence of about 1/487 on both side walls to correct for the sidewall boundary layer growth. A constant pressure boundary layer developed on a flat plate that was placed horizontally in the mid-plane of the test section. The plate leading edge had a super-ellipse shape (Narasimha and Prasad, 1994), which merged smoothly with the plate; this shape has been used in many constant pressure experiments (Narasimha and Prasad, 1994; Vasudevan et al, 2001; Banerjee et al, 2006).

The streamwise distance from the leading edge is denoted by x (Fig. 1) and the wall-normal and spanwise coordinates are y and z, respectively. The origin of the coordinate system is midspan at the plate leading edge. The single-vortex generator was a 2-dimensional hill with a Gaussian profile: $y_h(x) = h\exp[-((x-x_0)/a)^2]$, $(|x-x_0| \le C/2)$. It was made of Balsa and spanned from $z = 0$ to one sidewall of the tunnel, as shown in Fig. 1. It was affixed to the plate at a distance $x_0 = 275$ mm from the leading edge. Two hills were used, *shallow* and *steep* with the values listed in Table 1.

A constant-temperature hot-wire anemometer with a 5 micron tungsten wire as the sensing element was used. The length to diameter ratio of the hot-wire is about 400. The hot-wire was calibrated, before and after each experiment, using King's law. For the hot-wire measurements, the wall ($y = 0$) was identified following the procedure in Banerjee et al (2006).

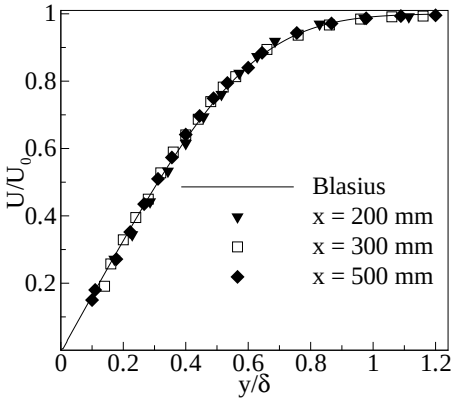

Figure 2: Streamwise velocity profiles without hill at $U_0 = 8$ m/s.

The PIV unit (IDTpiv, USA) consisted of a double cavity Nd:YAG laser (New Wave Res, 100 mJ), a CCD camera (Sharpvision 1400DE; 1360 × 1036 pixels) and the associated data processing software, proVISION. This data processing software was based on a second-order accurate mesh-free algorithm of Lourenco and Krothapalli (2000). In the double exposure mode, the camera could capture five image pairs per second. The flow was seeded by smoke particles ($\approx 1\mu$m; EUROLITE smoke fluid) generated by a commercial fog generator (HP Line), which was placed at about 3,000 mm ahead of the tunnel entry.

Without the vortex generator, a Blasius boundary layer was established over the plate. The mean streamwise velocity component is $U(x, y, z)$, and the freestream speed is U_0. Measurements at stations $x = 200$, 300 and 500 mm at a freestream speed of $U_0 = 8$ m/s, are shown in Fig. 2. Here, the boundary layer thickness δ corresponds to 0.99 U_0. At $x = 275$ mm, $\delta = 5.4$ mm and 3.7 mm at 3.5 m/s and 7.5 m/s, respectively. So the height of the vortex-generator is less than that of the incoming boundary layer which sweeps over it. The corresponding values of Re_θ $(= U_0\theta/\nu)$ based on momentum thickness θ were 168 and 245. In the following graphs distances are sometimes scaled with h, and sometimes with δ_0 which is then the thickness at $x_0 = 275$ mm, without the hill.

Vortex generation

There are two mechanisms for the origin of streamwise vorticity ω_x at the edge of the hill. One is the inviscid mechanism of tilting of the spanwise vorticity in the uniform, incoming boundary layer due to the spanwise velocity gradient. The second is from the crossstream pressure gradient and viscous diffusion of vorticity from the wall. Owing to the curvature of the hill, and therefore that of streamlines close to it, there is a pressure gradient normal to the streamlines. As the stream approaches the hill, initially the pressure near the hill surface rises over the concave windward part, then falls over the convex top, and then rises again near the trailing end of the hill. This implies a spanwise pressure gradient between the flow that passes over the hill and that which does not. Consistent with the pressure rise on the windward side is a deceleration and both the velocity gradient $\partial U/\partial z$ and the pressure gradient are positive near the hill's edge. Since $\omega_z < 0$, the streamwise vorticity due to the tilting is negative, while that due to viscous diffusion is positive. Near the convex top of the hill, both mechanisms give rise

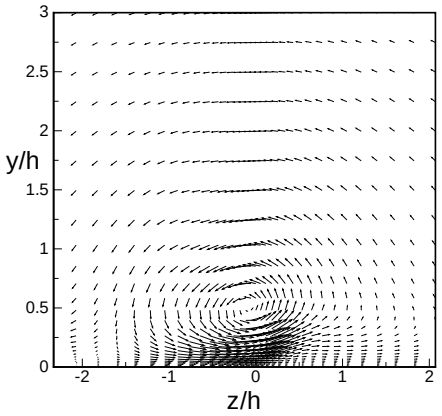

Figure 3: Crossflow velocity vectors from simulation. Steep hill, $U_0 = 7.5$ m/s, $x = 297.5$ mm.

to negative streamwise vorticity, while near the trailing edge, the signs are different again. What remains downstream is the net effect of these processes. Streamwise *vortices* can be identified when the streamwise vorticity rolls up downstream.

Since positive and negative streamwise vorticity are present the net effect cannot be deduced by argument alone, but the flow immediately downstream of the hill is readily obtained from laminar flow computations. The full flow requires more careful, DNS-quality, computations, because of the ensuing transition, and have not been undertaken in this study. Here, a commercially-available program FLUENT was used in the vicinity of the hill. The computational region was $-C < x - x_0 < 2C$, $0 < y < 15$ mm and $-C < z < C$. Conditions are close to those of the experiment. At inflow the Blasius profile was specified. At side and upper walls, slip flow was allowed, and extrapolation at the outflow plane. The grid was clustered close to the wall and near the edge of the hill. There were $200 \times 45 \times 60$ grid points in the streamwise, wall normal and spanwise directions for the shallow hill, and $120 \times 45 \times 60$ points for the steep hill.

Simulations were performed for the two hills at $U_0 = 3.5$ and 7.5 m/s. In all cases streamwise vorticity of both signs are found downstream but the rolled-up streamwise vortex is counterclockwise. Initially, on the windward side there is crossflow with spanwise velocity $W > 0$ above the hill giving $\omega_x > 0$. A little above the hill's edge ($z = 0$ plane), a pocket is present where $\omega_x < 0$, from tilting of spanwise vorticity. As the flow passes over the hill, the crossflow reverses near the hill surface so that $\omega_x < 0$ immediately above this surface while an extended layer with $\omega_x > 0$ lies over this. The cumulative effect is a crossflow with $\omega_x < 0$ near the plate surface and a single rolled-up counterclockwise streamwise vortex near $z = 0$ in all 4 cases. Figure 3 shows the streamwise vortex in the crossflow velocity vector plot with the steep hill at $x = 297.5$ mm ($C/4$ downstream of hill trailing edge).

RESULTS FROM EXPERIMENTS

The flow fields downstream of the shallow and steep hills were measured using PIV and hot-wire for freestream speeds U_0 of 3.5 m/s and 7.5 m/s. The PIV data provides velocity fields on several wall-parallel planes for $y > 1$ mm. Hot-wire data is available at locations closer to the wall. Measurements were over a wider extent than in Hamilton and Abernathy (1994) (only -1.7 $\leq z/h \leq$ 3.3; see their Fig. 9). The PIV data showed the development of streaks due to the streamwise vorticity. At the lower speed, streaks developed but flow did not transition even at the end of the measurement window, $x = 380$. At the higher speed transition was detected in the hot-wire data. The maximum value of the rms of streamwise velocity fluctuations u' at several downstream locations along $z = 0$ is shown in Fig. 4. With either hill, at the lower freestream speed there is very little growth in fluctuation level. At $U_0 = 7.5$ m/s, fluctuations grow to a peak level, then fall slightly but does not appear to decay significantly. With the steep hill the distribution is remarkably similar to that in K-type transition measurements of Klebanoff et al (1962), including the peak level of about 12% and the level of about 8% found downstream. Peak and sustained fluctuations were smaller for the shallow hill. Here the lower freestream speed case will be termed non-transitional to mean that the presence of the hill does not provoke a transition a short distance downstream; the boundary layer will eventually undergo transition sufficiently far downstream.

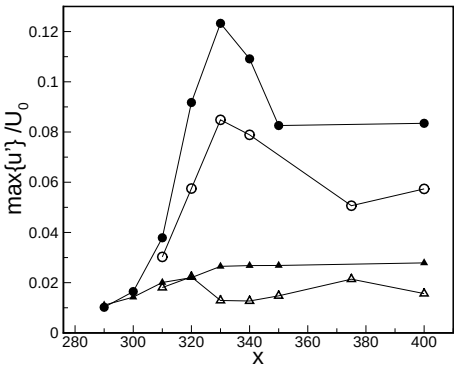

Figure 4: Maximum over the boundary layer at each station $x, z = 0$, of rms of streamwise velocity fluctuations. Empty symbols: shallow hill; filled: steep hill; circles: $U_0 = 7.5$ m/s; triangles: $U_0 = 3.5$ m/s. (Hot-wire data).

Low speed, non-transitional

At $U_0 = 3.5$ m/s, streaks form with little development downstream. Contours of the mean velocity $U(x, y/h = 1.52, z)$ showed two streaks a short distance downstream of the shallow hill. Several cross-stream profiles of velocity components U and W from the steep hill experiment at $x = 400$ are shown in Fig. 5 (some curves of $W(z)$ have been omitted for clarity). With the steep hill, the streaks were wider because the hill height was twice as large and the size of the streamwise vortex which creates the streaks scales with hill height. Mean velocity profiles $U(x, y, z = 0)$ show some deviations from the Blasius profile, notably, becoming inflectional, but does not suffer an instability to become full as in turbulent boundary layers (Fig. 6).

High speed, transitional

At the higher freestream speed, $U_0 = 7.5$ m/s, the flow undergoes more substantial changes resulting in transition, but the responses, or routes, are distinct for the two hills. With the steep hill the downstream development involves periodic fluctuations and growth of harmonics and eventual breakdown. With the shallow hill, such a progression through growth of harmonics was not identifiable, but flow breakdown occurred closer to the hill, and a turbulent sig-

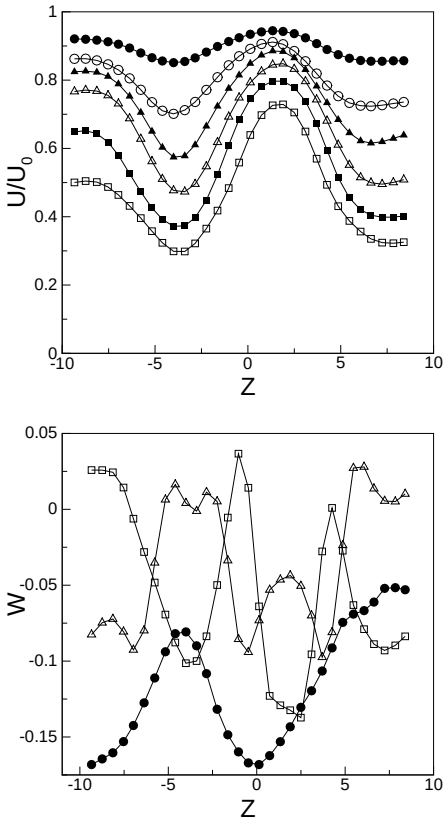

Figure 5: Profiles $U(z)$ and $W(z)$ at $x = 400$; steep hill, $U_0 = 3.5$ (PIV data). $y/h = 0.43$: □; 0.53 : ■; 0.66 : △; 0.836 : ▲; 0.99 : O; 1.24 : •

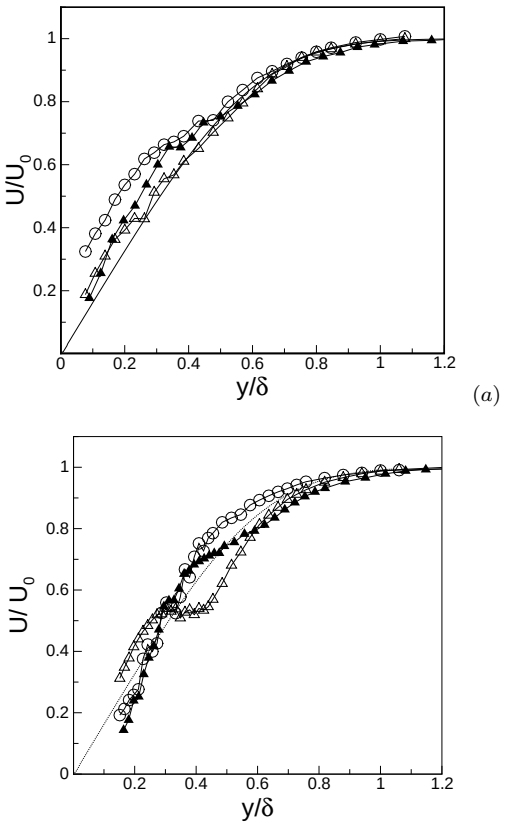

Figure 6: Profiles $U(y)$ for $U_0 = 3.5$ m/s. (a): shallow hill, at $x = 320$ mm (—△—), 350 mm (—▲—), 375 mm (–O–); (b): steep hill, at $x = 310$ mm (—△—), 330 mm (—▲—), 400 mm (–O–); Blasius (——). (Hot-wire data)

nal was obtained with a broad spectrum. These fluctuations originated closer to the wall and could not be detected in the PIV data which was limited to $y > 1$ mm.

The structure of the flow that forms just downstream of the hill is more complicated than that at the lower speed. Several streaks were present. With the steep hill, velocity profiles at $x = 310$ suggest the action of a strong counter-clockwise vortex on the $z > 0$ side of the steep hill (Fig. 7). Two low-speed streaks on the two sides of a high speed streak centered around $z \approx -2$ were seen, but the larger velocity deficit in the low speed streak in $z > 0$ diminishes downstream. With the shallow hill, the PIV data showed a pair of high-speed streaks flanked by a pair of low-speed ones, and all streaks undergo mild development downstream (Fig. 8). Some variations along the high speed streaks were evident in the PIV data of instantaneous velocity fields. However, the hot-wire data (discussed below) showed flow to undergo a rapid and continuous breakdown, close the wall and within a short distance of the shallow hill.

Some differences in the transition route are evident in wall-normal profiles $U(y)$ (Fig. 9). With the shallow hill, the profile had distorted, becoming inflectional at $x = 320$ mm. By $x = 340$ mm it had become fuller close to the wall and then developed monotonically to flat turbulent profiles. With the steep hill, the initial distortion at $x = 310$ was similar, but then a near-uniform region appeared over $0.15 < y/\delta < 0.5$, before eventually tending to a flat turbulent shape.

Qualitative differences in the route to transition become evident in hot-wire signals and spectra. With the steep hill, there are periodic fluctuations with a primary frequency of 386 Hz and harmonics. Though the peak is quite sharp, there is a sideband indicating a modulation. At $x = 330$ mm, the primary and the first harmonic are dominant. The sideband is also similar. At $x = 400$ a turbulent signal is obtained and the spectrum is broad; a peak at 386 Hz is still clear, but harmonics are less distinct (Fig 10). By $x = 450$ mm the primary peak has also disappeared. Time series of the hot-wire voltage e' shows the appearance of the wavepacket, its growth and eventual breakdown into turbulence. In Fig 12 time series at the location of the maximum

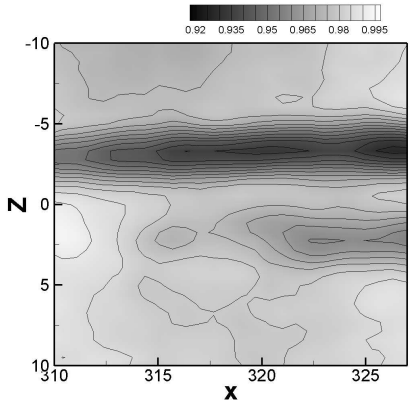

Figure 7: Contours of mean streamwise component U at $y/h = 0.75$; steep hill, $U_0 = 7.5$ (PIV data)

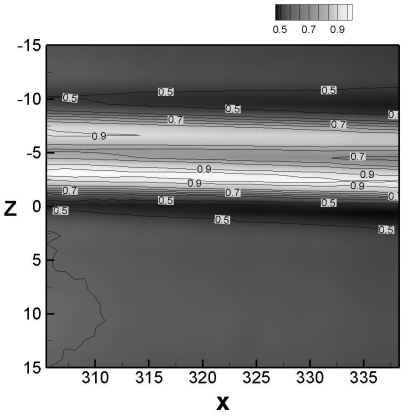

Figure 8: Contours of mean streamwise component U at $y/h = 1.64$; shallow hill, $U_0 = 7.5$ m/s(PIV data)

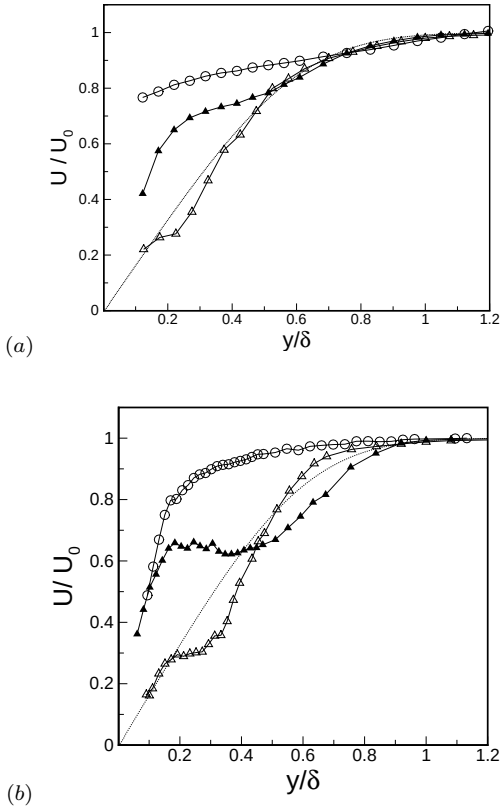

Figure 9: Profiles $U(y)$ for $U_0 = 7.5$ m/s. (a): shallow hill, at $x = 320$ mm (—△—), 340 mm (—▲—), 400 mm (–O–); (b): steep hill, at $x = 310$ mm (—△—), 330 mm (—▲—), 400 mm (–O–); Blasius (——). (Hot-wire data)

fluctuations are shown. Similar time series with the shallow hill do not show a wave packet before transition (Fig 13). The spectra are more clearly broadband every where, continuously developing to the turbulent state (Fig 11).

Klebanoff et al (1992) found the a dimensionless frequency parameter to be about 0.3 in their experiments with an isolated cylinder model of roughness. They attributed the frequency to oscillations of the vortex forming around the cylinder. Using their scaling, the peak $f = 386$ Hz obtained with the steep hill makes the dimensionless frequency parameter $2\pi f\delta_h^*/U_h = 0.46$; δ_h^* to be the is the displacement thickness at the roughness location (here, hill peak)

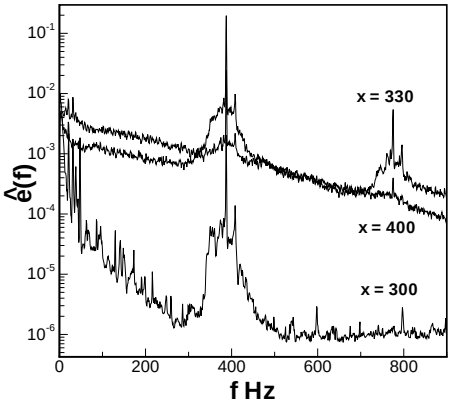

Figure 10: Fourier transform of hot-wire voltage, steep hill at $U_0 = 7.5$ m/s at $x = 300$, 330, 400 mm.

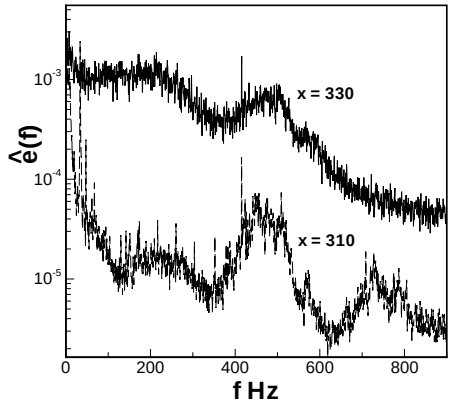

Figure 11: Fourier transform of hot-wire voltage, shallow hill at $U_0 = 7.5$ m/s at $x = 310$, 330 mm.

and U_h is the velocity at the roughness height in the undisturbed flow. The straightforward scaling, $2\pi fh/U_0 = 0.97$, suggests that the frequency peak is due to an inviscid mechanism that persists far downstream ($x = 400$ mm is $42h$ from the hill center) even while the flow breaks down and frequency content grows over a range of scales. These differences in the time series suggest that the thicker vortex induced by the steep hill exhibits a vortex or streak instability before a later stage of breakdown, whereas this latter stage appears immediately downstream of the shallow hill. The difference may be due to the vortex induced by the shallow hill being closer to the wall, and wall interaction of the streamwise vortex being the essential final stage.

SUMMARY AND CONCLUSIONS

Computations have shown that the streamwise vorticity induced by the spanwise asymmetry of the hill rolls up into a single streamwise vortex. Experiments show this vortex to undergo an instability resulting in oscillations at a frequency which scales on inviscid parameters. Further instability results in transition to turbulence. When the vortex is close to the wall, these oscillations are not distinct and the flow breaks down to turbulence quickly. It remains to be determined how the vortex instability downstream of the steep hill develops into a closer interaction with the wall and any common features of that stage with that of the shallow hill transition.

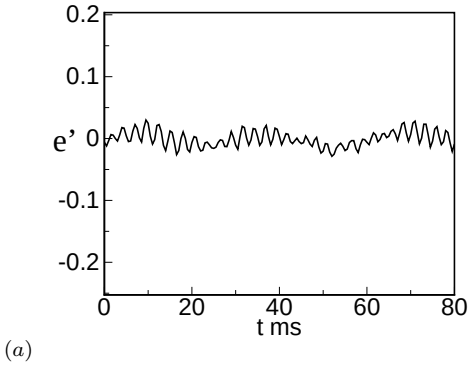

(*a*)

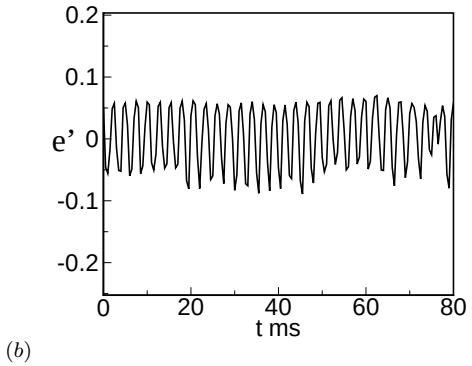

(*b*)

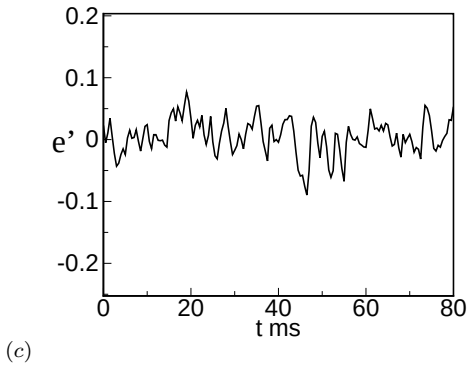

(*c*)

Figure 12: Time series of hot-wire voltage, steep hill at $U_0 = 7.5$ m/s at $x = 310$, 330, 400 mm, (a, b, c).

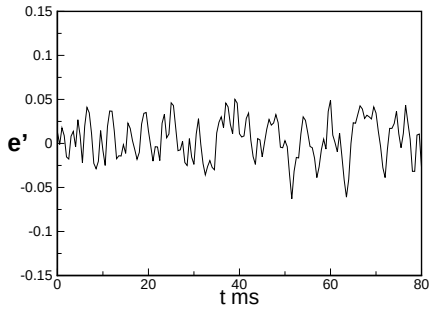

Figure 13: Time series of hot-wire voltage, shallow hill at $U_0 = 7.5$ m/s at $x = 330$.

*

REFERENCES

Acarlar MS, Smith CR (1987) A study of hairpin vortices in a laminar boundary layer. Part 1. Hairpin vortices generated by a hemisphere protuberance. J Fluid Mech 175:1–41

Asai M, Minagawa M, Nishioka M (2002) The instability and breakdown of a near-wall low-speed streak. J Fluid Mech 182:255–290

Bakchinov AA, Grek GR, Klingmann BGB, Kozlov VV (1995) Transition experiments in a boundary layer with embedded streamwise vortices. Phys Fluids 7(820):820–832

Banerjee AS, Mandal AC, Dey J (2006) Particle image velocimetry studies of an incipient spot in the Blasius boundary layer. Exp Fluids 40(6):928–940

Durbin P, Wu XH (2007) Transition beneath vortical disturbances. Ann Rev Fluid Mech 39:107–128

Hamilton JM, Abernathy FH (1994) Streamwise vortices and transition to turbulence. J Fluid Mech 264:185–212

Kachanov YS (1994) Physical mechanisms of laminar-boundary-layer transition. Ann Rev Fluid Mech 26:411–482

Klebanoff PS, Tidstrom KD, Sargent LM (1962) The three dimensional nature of boundary-layer instability. J Fluid Mech 12(1):1–34

Klebanoff PS, Cleveland WG, Tidstrom ISD (1992) On the evolution of a turbulent boundary layer induced by a three-dimensional roughness element. J Fluid Mech 237:101–187

Lourenco LM, Krothapalli A (2000) TRUE resolution PIV: a mesh-free second order accurate algorithm. In: Proceedings of the International Conference in applications of lasers to fluid mechanics

Narasimha R, Prasad SN (1994) Leading edge shape for flat plate boundary layer studies. Exp Fluids 17(5):358–360

Saric WS, Reed HL, Kerschen EJ (2002) Transition beneath vortical disturbances. Ann Rev Fluid Mech 34:291–319

Swearingen JD, Blackwelder RF (1987) The growth and breakdown of streamwise vortices in the presence of a wall. J Fluid Mech 182:255–290

Vasudevan KP, Dey J, Prabhu A (2001) Spot propagation characteristics in laterally strained boundary layers. Exp Fluids 30(5):488–491